INSTITUTE OF PHYSICS PUBLISHING JOURNAL OF OPTICS A: PURE AND APPLIED OPTICS
J. Opt. A: Pure Appl. Opt. **6** (2004) 259–268 PII: S1464-4258(04)68948-3

Optical vortices evolving from helicoidal integer and fractional phase steps

M V Berry

H H Wills Physics Laboratory, Tyndall Avenue, Bristol BS8 1TL, UK

Received 10 September 2003, accepted for publication 8 January 2004
Published 26 January 2004
Online at stacks.iop.org/JOptA/6/259 (DOI: 10.1088/1464-4258/6/2/018)

Abstract
The evolution of a wave starting at $z = 0$ as $\exp(\mathrm{i}\alpha\phi)$ $(0 \leqslant \phi < 2\pi)$, i.e. with unit amplitude and a phase step $2\pi\alpha$ on the positive x axis, is studied exactly and paraxially. For integer steps ($\alpha = n$), the singularity at the origin $\mathbf{r} = 0$ becomes for $z > 0$ a strength n optical vortex, whose neighbourhood is described in detail. Far from the axis, the wave is the sum of $\exp\{\mathrm{i}(\alpha\phi + kz)\}$ and a diffracted wave from $\mathbf{r} = 0$. The paraxial wave and the wave far from the vortex are incorporated into a uniform approximation that describes the wave with high accuracy, even well into the evanescent zone. For fractional α, no fractional-strength vortices can propagate; instead, the interference between an additional diffracted wave, from the phase step discontinuity, with $\exp\{\mathrm{i}(\alpha\phi + kz)\}$ and the wave scattered from $\mathbf{r} = 0$, generates a pattern of strength-1 vortex lines, whose total (signed) strength S_α is the nearest integer to α. For small $|\alpha - n|$, these lines are close to the z axis. As α passes $n + 1/2$, S_α jumps by unity, so a vortex is born. The mechanism involves an infinite chain of alternating-strength vortices close to the positive x axis for $\alpha = n + 1/2$, which annihilate in pairs differently when $\alpha > n + 1/2$ and when $\alpha < n + 1/2$. There is a partial analogy between α and the quantum flux in the Aharonov–Bohm effect.

Keywords: vortices, singularities, asymptotics, phase

1. Introduction

Spiral phase plates, that is, refracting or reflecting surfaces shaped into one turn of a helicoid, with the pitch of the helicoid chosen to generate a prescribed phase step, are common devices for creating screw-dislocated waves [1, 2]. The first example known to me was made in the late 1970s from cardboard, and used to make a dislocation in ultrasound [17]. It is clearly desirable to have a good description of the optical vortices (dislocations, or lines of phase singularity) in the wave beyond a spiral phase plate. Here I explore in detail a model that is realistic enough to capture the essential singularity structure, yet simple enough to be analytically tractable.

The model is the propagation into the space $z > 0$ of a wave that starts from the plane $z = 0$ with a phase singularity of strength $2\pi\alpha$, and unit amplitude. With coordinates (figure 1)

$$\mathbf{r} = \{x, y, z\}, \qquad \mathbf{R} = \{x, y\} = R\{\cos\phi, \sin\phi\}, \qquad \boldsymbol{\rho} = \mathbf{R}/\sqrt{z} = \{\xi, \eta\} \tag{1}$$

(where $\boldsymbol{\rho}$, ξ and η are defined for later use), the initial wave is

$$\Psi_\alpha(\mathbf{R}, 0) = \exp(\mathrm{i}\alpha\phi) \qquad (0 \leqslant \phi < 2\pi). \tag{2}$$

Thus, the phase increases by $2\pi\alpha$ in a circuit of the origin, with a step discontinuity of phase along the positive x axis $\xi = 0$. The distinction between integer and fractional α will be important.

A real phase plate where the phase step is associated with a height step will exhibit some diffraction phenomena not captured by this model. For example, there will be multiple scattering of waves diffracted by the edges of the step. This is a hard problem, even for an infinite step; but preliminary computations, carried out for an infinite mirror step as an analogue of the Aharonov–Bohm effect ([3]—see also section 4), suggest that the main features are captured by modelling the height step with a phase step, provided α is not too large. Moreover, spiral phase plates are commonly illuminated not by plane waves but by beams (e.g. Gaussian) of finite width [4, 5]; such beams are easy to simulate numerically [2], and can easily be incorporated into the

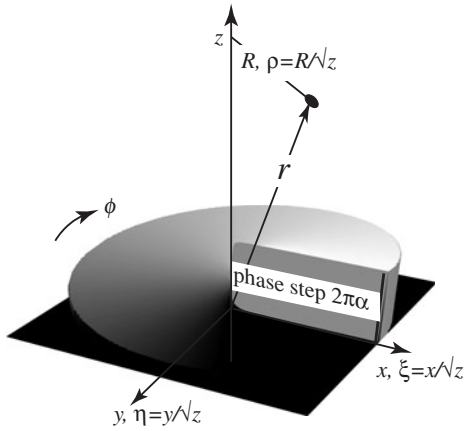

Figure 1. Notation and coordinates for a helicoidal phase step.

analytical theory, as described briefly below. The effects of finite width will be studied in detail elsewhere, since the model (2) already contains a rich structure of optical vortices, worth exploring for its own sake.

Section 2 is devoted to the case where α is an integer n. The wave (2) does not vanish at $\mathbf{R} = 0$, where the phase singularity creates a point discontinuity that must be smoothed away during propagation to $z > 0$. In fact there is a screw dislocation along the z axis $\mathbf{R} = 0$, at which Ψ vanishes like $C(z)R^n$.

Section 3 deals with the case where α is not an integer. Then the initial wave (2) contains not only a fractional-order singularity at $\mathbf{R} = 0$ but also a step discontinuity along the positive x axis, which must also be healed by propagation to $z > 0$. Of course, vortices with fractional strength cannot propagate in free space [4]; instead, the step at $z = 0$ breaks up into a collection of strength ± 1 vortices [5], in an intricate arrangement, described in detail, with interesting interactions as α increases through half-integer values. Section 4 describes a curious analogy between diffraction from helicoidal phase steps and the Aharonov–Bohm effect [6] of quantum mechanics.

Since there is no scale other than the wavelength λ of the propagating wave, we will measure all distances in units of $\lambda/2\pi$; this is equivalent to choosing the wavenumber $k = 1$.

2. Integer phase steps

2.1. Exact and paraxial waves for integer α

The wave for $z \geqslant 0$ can be written as a superposition of plane waves with transverse wavevectors $\mathbf{K} = \{K_x, K_y\} = K\{\cos\phi_{\mathbf{K}}, \sin\phi_{\mathbf{K}}\}$. Thus, for $\alpha = n$,

$$\Psi_n(\mathbf{r}) = \int\!\!\int_{\mathbf{K}\ \text{plane}} \mathrm{d}\mathbf{K}\, a_n(\mathbf{K}) \exp\left\{\mathrm{i}\left(\mathbf{R}\cdot\mathbf{K} + z\sqrt{1-K^2}\right)\right\}. \tag{3}$$

The waves with $K > 1$ are evanescent, and, as has been emphasized recently [7], they must be included because their existence is an inevitable consequence of the singularity in (2). Fourier transformation of (2) for $\alpha = n$ gives the plane-wave amplitudes $a_n(\mathbf{K})$:

$$a_n(\mathbf{K}) = \frac{1}{4\pi^2}\int\!\!\int_{\mathbf{R}\ \text{plane}} \mathrm{d}\mathbf{R} \exp\{\mathrm{i}(\mathbf{K}\cdot\mathbf{R} + n\phi)\}$$

$$= \frac{|n|(-\mathrm{i})^{|n|}}{2\pi K^2}\exp(\mathrm{i}n\phi_{\mathbf{K}}). \tag{4}$$

The propagating wave is thus

$$\Psi_n(\mathbf{r}) = \exp(\mathrm{i}n\phi)|n|\int_0^\infty \frac{\mathrm{d}K}{K} J_{|n|}(KR)\exp\left(\mathrm{i}z\sqrt{1-K^2}\right), \tag{5}$$

where $J_{|n|}$ denotes the Bessel function of the first kind.

In the paraxial approximation, where $\sqrt{(1-K^2)}$ is replaced by $1 - K^2/2$, the wave, now denoted ψ (in contrast to the exact wave Ψ) becomes

$$\psi_n(\mathbf{r}) = \exp\{\mathrm{i}(n\phi + z)\}|n|\int_0^\infty \frac{\mathrm{d}K}{K} J_{|n|}(KR)\exp\left(-\frac{1}{2}\mathrm{i}zK^2\right)$$

$$= \exp\{\mathrm{i}(n\phi + z)\}P_n\left(\frac{R}{\sqrt{z}}\right). \tag{6}$$

By manipulating standard Bessel integrals, P_n (not to be confused with the Legendre polynomial) can be evaluated analytically, with the result

$$P_n(\rho) = \sqrt{\frac{\pi}{8}}(-\mathrm{i})^{|n|/2}\rho\exp\left(\frac{1}{4}\mathrm{i}\rho^2\right)$$
$$\times\left[J_{\frac{1}{2}(|n|-1)}\left(\tfrac{1}{4}\rho^2\right) - \mathrm{i}J_{\frac{1}{2}(|n|+1)}\left(\tfrac{1}{4}\rho^2\right)\right]. \tag{7}$$

Because of the scaling in (6), the pattern of ψ_n as a function of R is the same for all z, up to dilation. (It is worth noting that for even n the formula (7) involves Bessel functions of half-integer order, which can be expressed as finite trigonometric sums.)

If the phase step is illuminated by a Gaussian beam of width w (that is, with initial wave profile $\exp(-R^2/2w^2)$) instead of a plane wave, it is easy to show that the only effect on the paraxial wave is to replace ρ^2 in the square brackets in (7) by $\rho^2/(1 + \mathrm{i}z/w^2)$ and multiply P_n by $1/\sqrt{(1 + \mathrm{i}z/w^2)}$. The consequences of this (more serious for fractional α than integer α) will be explored elsewhere.

Figure 2 shows the exact amplitude $|\Psi_1|$ and the paraxial amplitude $|\psi_1|$ for the simplest vortex wave, as functions of R for several fixed values of z. The paraxial approximation works well near the vortex, but gives an accurate description of the oscillations far from the vortex only when $z \gg 1$ and $R/z \ll 1$, as expected.

Figure 3 shows the wavefronts $\arg\psi_n = \text{constant}$, for the paraxial wave $n = 3$. They spiral out from the phase singularity at the vortex, and then issue radially asymptotically straight out to infinity like the initial wavefronts (2), with an oscillatory decoration. The exact wavefronts $\arg\Psi_n$ are similar, except that the asymptotic oscillations are slightly different, as we will see later.

2.2. Near the z axis

The singularity of (2) at $\mathbf{R} = 0$ is immediately healed by propagation to $z > 0$. To study this in detail, we can approximate the wave near $\mathbf{R} = 0$. From (5),

$$\Psi_n(\mathbf{R}\to 0, z)$$
$$= \exp(\mathrm{i}n\phi)\frac{|n|R^{|n|}}{2^{|n|}\Gamma(|n|+1)}\int_0^\infty \mathrm{d}K\, K^{|n|-1}\exp\left(\mathrm{i}z\sqrt{1-K^2}\right)$$
$$= \exp(\mathrm{i}n\phi)\frac{\mathrm{i}\pi R^{|n|}}{2^{\frac{1}{2}(3|n|+1)}\Gamma(\frac{1}{2}(|n|+1))z^{\frac{1}{2}(|n|-1)}}H^{(1)}_{\frac{1}{2}(|n|+1)}(z), \tag{8}$$

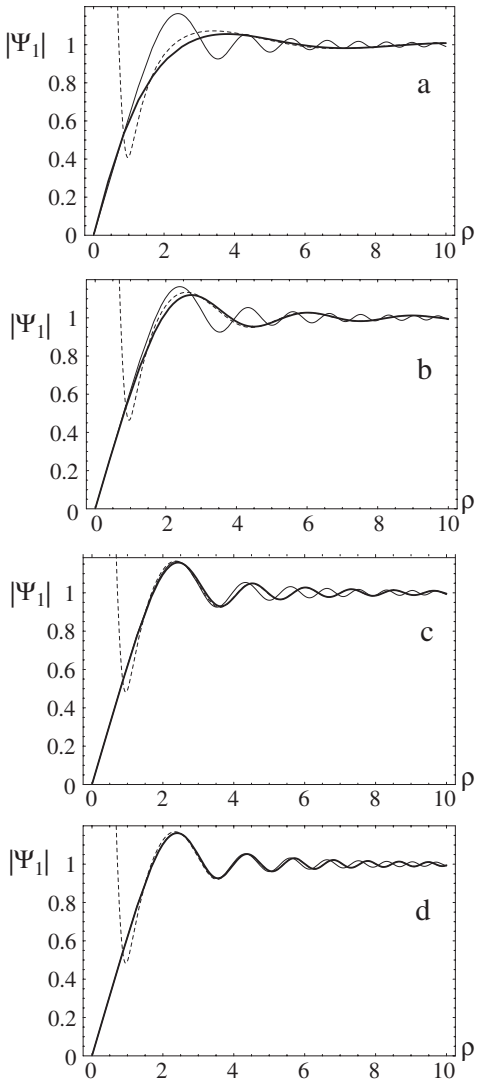

Figure 2. The wave modulus for $\alpha = 1$ as a function of the paraxial variable $R/\sqrt{z}$, for (a) $z = 1$; (b) $z = 5$; (c) $z = 50$; (d) $z = 200$. Thick curve, exact wave $|\Psi_1|$ (5); thin curve, paraxial wave $|\psi_1|$ (7); dashed curve, geometrical approximation (11).

where $H_\nu^{(1)}$ denotes the Bessel function of the third kind. This shows that Ψ_n vanishes as R^n on the z axis, with a coefficient that diverges as z^{-n} as $z \to 0$.

The paraxial wave (7) also vanishes at $\mathbf{R} = 0$, as

$$P_n(\rho \to 0) = \sqrt{\pi}\left(\frac{-\mathrm{i}}{8}\right)^{\frac{1}{2}|n|} \frac{\rho^{|n|}}{\Gamma(\frac{1}{2}(|n|+1))}. \tag{9}$$

The asymptotic form of $H_\nu^{(1)}$ in (8) shows that the exact and paraxial coefficients of R^n become equal for large z. However, the paraxial divergence as $z \to 0$ is weaker—diverging as $z^{-n/2}$ rather than z^{-n}—an unsurprising difference in this nonparaxial evanescent zone.

It is worth digressing briefly to follow [7] and investigate a third form of the wave near the z axis, namely that which would propagate from the initial wave (2) with its evanescent components $K < 1$ deleted. This is

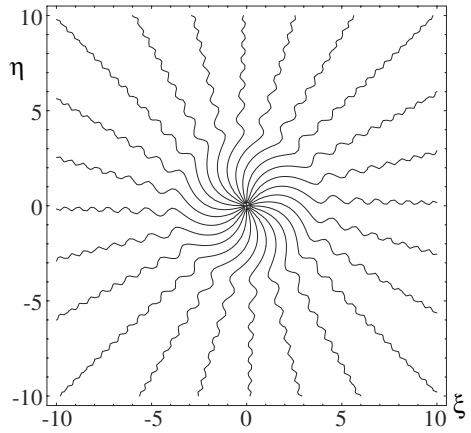

Figure 3. Paraxial wavefronts $\arg\psi = \text{constant}$ (from (7)) at phase intervals of $\pi/4$, for $\alpha = 3$.

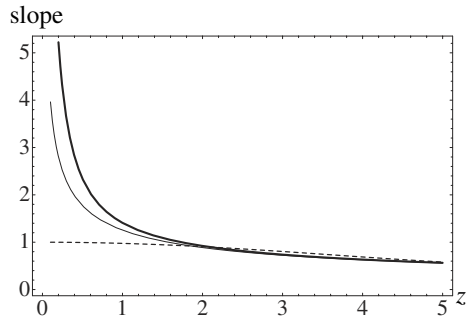

Figure 4. The slope $\partial|\Psi|/\partial R$ at $R = 0$, for $\alpha = 1$. Thick curve, exact wave (8); thin curve, paraxial wave (9); dashed curve, nonevanescent contribution (10).

$$\begin{aligned}
&\Psi_{n,\text{nonevanescent}}(\mathbf{R} \to 0, z) \\
&= \exp(\mathrm{i}n\phi)\frac{R^{|n|}}{2^{|n|}\Gamma(|n|+1)}\int_0^1 \mathrm{d}K\, K^{|n|-1}\exp\bigl(\mathrm{i}z\sqrt{1-K^2}\bigr) \\
&= \exp(\mathrm{i}n\phi)\frac{\mathrm{i}\pi R^{|n|}}{2^{\frac{1}{2}(3|n|+1)}\Gamma(\frac{1}{2}(|n|+1))z^{\frac{1}{2}(|n|-1)}} \\
&\quad\times\left[J^{(1)}_{\frac{1}{2}(|n|+1)}(z) + \mathrm{i}\left(\mathrm{H}_{\frac{1}{2}(|n|+1)}(z)\right.\right. \\
&\quad\left.\left. - \frac{z^{\frac{1}{2}(|n|-1)}}{\sqrt{\pi}2^{\frac{1}{2}(|n|-1)}\Gamma(\frac{1}{2}|n|+1)}\right)\right],
\end{aligned} \tag{10}$$

where H_ν denotes the Struve function.

Figure 4 shows the coefficients (factors multiplying R^n) of all three waves for the simplest singularity $n = 1$. All curves agree for large z, and the paraxial approximation works surprisingly well, even into the evanescent zone $z \sim 1$, corresponding to a distance $\lambda/2\pi$ from the initial singularity. Of course, the nonevanescent wave fails to describe the approach to the singularity for small z.

2.3. Geometrical approximation away from the z axis

For $z \gg 1$ and also away from the axis, that is for $R \gg 1$, the wave (5) can be approximated, in the spirit of the geometrical theory of diffraction [8], as the sum of two contributions: from the neighbourhoods of $K = 0$ and from the stationary point (after approximating J_n) at $K = R/\sqrt{(z^2+R^2)}$. For the first

contribution, we use $\int_0^\infty \mathrm{d}K\, J_n(KR)/K = 1/n$, and for the second we use the method of stationary phase. The result is

$$\Psi_{n,\mathrm{geom}}(\mathbf{r}) = \exp(\mathrm{i}n\phi)\left[\exp(\mathrm{i}z) - \frac{\mathrm{i}|n|z}{R^2}(-\mathrm{i})^n \exp(\mathrm{i}r)\right]. \tag{11}$$

The first term dominates. It represents the initial wave (2), propagated geometrically, including its singularity, with the factor $\exp(\mathrm{i}z)$. Together with (9), it explains the $\pi/4$ rotation of the wavefronts (figure 3) between $R = 0$ and ∞.

The second term in (11) can be regarded as a wave diffracted from the initial singularity at $r = 0$; the unfamiliar obliquity factor z/R^2 diverges not only at $r = 0$ but also on the vortex $R = 0$. The interference between the two contributions gives rise to the oscillations evident in Ψ_1 in figure 2, which also shows that (11), unlike the paraxial approximation, does reproduce the oscillations accurately.

2.4. Uniform approximation for Ψ_1

The anticipated failure of paraxiality for large R can be understood in detail by asymptotically approximating the Bessel functions in (7). The geometrically propagated wave comes from the lowest-order large-argument approximations, and the wave diffracted by the singularity comes from the first correction term. This gives

$$P_n(\rho \gg 1) = 1 - \frac{\mathrm{i}|n|}{\rho^2}(-\mathrm{i})^{|n|}\exp\left(\frac{1}{2}\mathrm{i}\rho^2\right), \tag{12}$$

which can also be obtained from (11) by the paraxial replacement $r \to z + R^2/2z$. The interference between the two terms gives rise to the asymptotic ripples visible in the modulus in figure 2 and the wavefronts in figure 3.

Although paraxiality fails for large R, this approximation is accurate near the vortex, and it does predict oscillations with the correct qualitative character. These observations can be exploited to obtain an approximation uniformly valid for large r both near and far from the vortex, by appropriately deforming the paraxial wave. The techniques for accomplishing this deformation are well established mathematically [9, 10], and have been widely applied to describe waves near and far from geometrical caustics [11, 12]. The present application has some resemblance to glory scattering [13], because of the circular symmetry, but has the unfamiliar feature that the failure of the geometrical approximation (11) occurs when the scattered contribution diverges not on a caustic but on the vortex.

The derivation of the uniform approximation for $n = 1$ is outlined in appendix A. The result is

$$\Psi_{1,\mathrm{uniform}}(\mathbf{r}) = \exp\left\{\mathrm{i}\left(\phi + z + B - \frac{1}{4}\pi\right)\right\}\frac{Rz\sqrt{2\pi}}{4} \times [p_0 J_0(B) - \mathrm{i}p_1 J_1(B) - p_2 J_2(B)], \tag{13}$$

where

$$B = \tfrac{1}{2}(r - z), \qquad p_0 = \frac{\sqrt{B}(3R^2 + 4zB)}{2R^3 z}, \qquad p_1 = \frac{2\sqrt{B}}{Rz}, \qquad p_2 = p_1 - p_0. \tag{14}$$

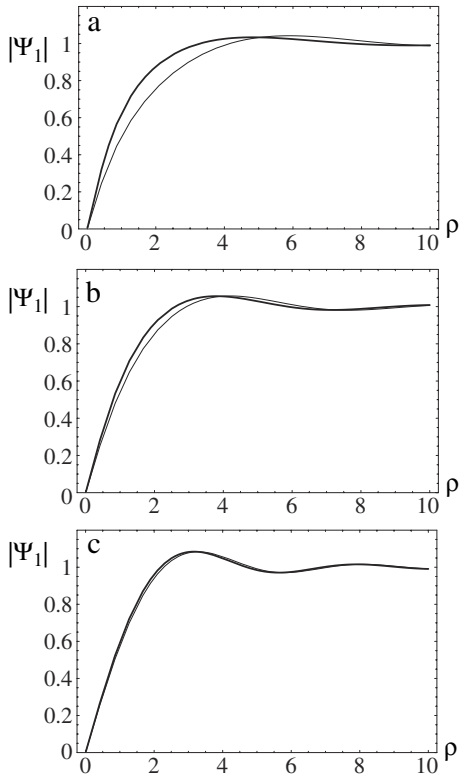

Figure 5. The modulus $|\Psi_1|$ as a function of the paraxial variable $R/\sqrt{z}$, for (a) $z = 0.5$; (b) $z = 1$; (c) $z = 2$. Thick curve, exact wave (5); thin curve, uniform approximation (13).

As figure 5 shows, this amalgamation of the paraxial and geometrical approximations is extraordinarily accurate, even for $z = 1/2$, corresponding to a distance $\lambda/4\pi = 0.08\lambda$ from the initial plane.

3. Fractional phase steps

3.1. Exact and paraxial waves for fractional α

When α is not an integer, the initial wave (2) possesses not only the singularity at $r = 0$ but also a step discontinuity along the positive x axis $\phi = 0$. But the propagating wave $\Psi_\alpha(\mathbf{r})$ must be smooth for $z > 0$, and is expressible as a superposition of the waves (5) for integer α. The resulting wave cannot contain fractional-strength vortices, but rather an arrangement of integer-strength vortices which we seek to determine.

The superposition is determined by the Fourier series

$$\exp(\mathrm{i}\alpha\phi) = \frac{\exp(\mathrm{i}\pi\alpha)\sin(\pi\alpha)}{\pi}\sum_{-\infty}^{\infty}\frac{\exp(\mathrm{i}n\phi)}{\alpha - n}. \tag{15}$$

Thus

$$\Psi_\alpha(\mathbf{r}) = \frac{\exp(\mathrm{i}\pi\alpha)\sin(\pi\alpha)}{\pi}\sum_{-\infty}^{\infty}\frac{\Psi_n(\mathbf{r})}{\alpha - n}. \tag{16}$$

The corresponding paraxial wave is

$$\psi_\alpha(\mathbf{r}) = \frac{\exp\{\mathrm{i}(z + \pi\alpha)\}\sin(\pi\alpha)}{\pi}\sum_{-\infty}^{\infty}\frac{\exp(\mathrm{i}n\phi)P_n(\rho)}{\alpha - n}, \tag{17}$$

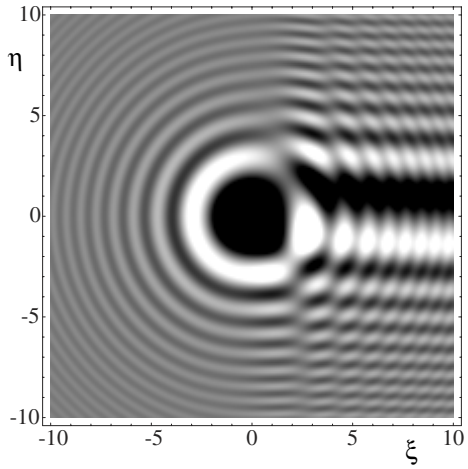

Figure 6. A density plot of the paraxial wave $|\psi_{\alpha=2.2}|$ in the ξ, η plane, calculated from (17).

where $P_n(\rho)$ is given by (7). From now on, we will work only with this paraxial wave, which contains all the essential geometric features.

An immediate consequence of (17) is that for fractional α there is no vortex on the z axis, where the only nonzero contribution to the sum comes from $P_0 = 1$, so that

$$\psi_\alpha(\mathbf{R} = 0, z) = \frac{\exp\{\mathrm{i}(z + \pi\alpha)\}\sin(\pi\alpha)}{\pi\alpha}. \tag{18}$$

Figure 6 shows a density plot of the modulus $|\psi|$, for $\alpha = 2.2$. This shows: low intensity near the z axis (even though there is no vortex on the axis itself); a dark stripe near the positive x axis; circular fringes surrounding $R = 0$, corresponding to diffraction by the singularity at the origin; and fringes parallel to the positive x axis, corresponding to waves diffracted by the step.

These interference effects can be understood in detail with the aid of the following uniform asymptotic formula, derived in appendix B, that is valid for $\xi \gg 0$ for all values of η including the positive ξ axis $\eta = 0$:

$$\begin{aligned}\psi_\alpha(\mathbf{r}) &\underset{\xi\gg 0}{\approx} \exp\{\mathrm{i}(z + \alpha(\phi + \pi))\} \\ &\times \left\{\cos\alpha\pi - \mathrm{i}\sin\alpha\pi\ \mathrm{erf}\left(\tfrac{1}{2}\eta\sqrt{1-\mathrm{i}}\right)\right. \\ &+ \sqrt{\frac{2}{\pi}}\frac{\exp\{\mathrm{i}(\frac{1}{2}\eta^2 - \frac{1}{4}\pi)\}\sin\alpha\pi}{\eta}(1 - \exp(-\mathrm{i}\alpha\phi)) \\ &\left. - \frac{\mathrm{i}\alpha}{\rho^2}\exp\left\{\mathrm{i}\left(\frac{1}{2}(\rho^2 + \pi\alpha)\right)\right\}\right\}. \end{aligned} \tag{19}$$

This formula (in which erf denotes the error function) will be used extensively in the following. It is very accurate. Visually, its reproduction of the right-hand side of figure 6 is indistinguishable from the original. Further illustrations are given in figure 7.

Physically, the terms in the first three lines of the formula (19) describe the spirally phased plane wave together with diffraction from the phase step along the positive ξ axis. These two effects merge near the axis (small $|\eta|$), as described by erf, but separate for large $|\xi|$, as can be seen from the first

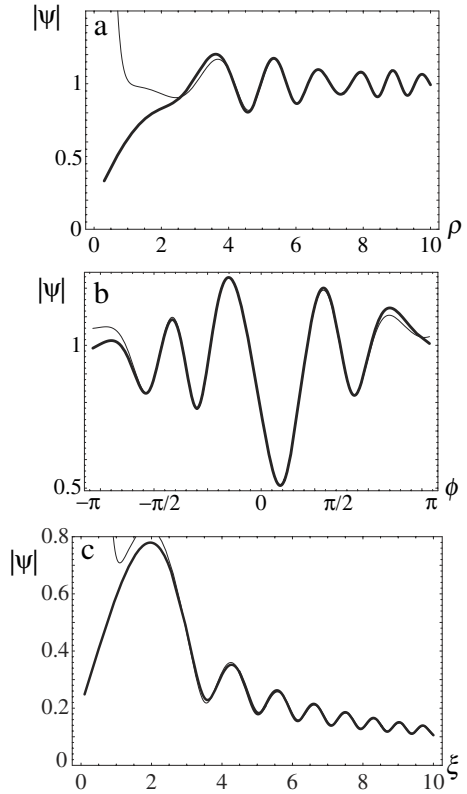

Figure 7. The accuracy of the uniform approximation (19). The modulus $|\psi_\alpha(r)|$ of the paraxial wave for $\xi > 0$: (a) radial plot, $\alpha = 1.25$, $\phi = \pi/3$; (b) angular plot, $\alpha = 1.25$, $\rho = 5$; (c) along the ξ axis, $\alpha = 3/2$, $\phi = 0$. Thick curves, paraxial wave (17); thin curves, asymptotic approximation (19) (also (28) for figure (c)).

line of the following formula obtained from (19) using the asymptotics of erf:

$$\begin{aligned}\psi_\alpha(\mathbf{r}) &\underset{\xi,|\eta|\gg 0}{\approx} \exp\{\mathrm{i}z\}\left\{\exp(\mathrm{i}\alpha\phi)\right. \\ &- \sqrt{\frac{2}{\pi}}\frac{\exp\{\mathrm{i}(\frac{1}{2}\eta^2 - \frac{1}{4}\pi)\}\sin\alpha\pi}{\eta} \\ &\left. - \frac{\mathrm{i}\alpha}{\rho^2}\exp\left\{\mathrm{i}\left(\frac{1}{2}\rho^2 + \alpha\left(\phi + \frac{3}{2}\pi\right)\right)\right\}\right\}. \end{aligned} \tag{20}$$

The term in the fourth line of (19), or in the third line of (20), describe waves diffracted from the singular point $\mathbf{r} = 0$ of the initial wave.

For integer α, there is no singularity at the edge and so there are no edge-diffracted waves, and (19) reproduces (12).

3.2. Total singularity strength

Although ψ_α has no vortex on the z axis, it does possess an interesting singularity structure. The total vortex strength is the signed sum of all the vortices threading a large loop including the z axis, namely

$$\begin{aligned}S_\alpha &= \lim_{R\to\infty}\frac{1}{2\pi}\int_0^{2\pi}\mathrm{d}\phi\,\frac{\partial}{\partial\phi}\arg\psi_\alpha(\mathbf{r}) \\ &= \lim_{\rho\to\infty}\frac{\mathrm{Re}}{2\pi}\int_0^{2\pi}\mathrm{d}\phi\,\frac{\sum_{-\infty}^{\infty}\frac{n}{n-\alpha}P_n(\rho)\exp(\mathrm{i}n\phi)}{\sum_{-\infty}^{\infty}\frac{1}{n-\alpha}P_n(\rho)\exp(\mathrm{i}n\phi)}. \end{aligned} \tag{21}$$

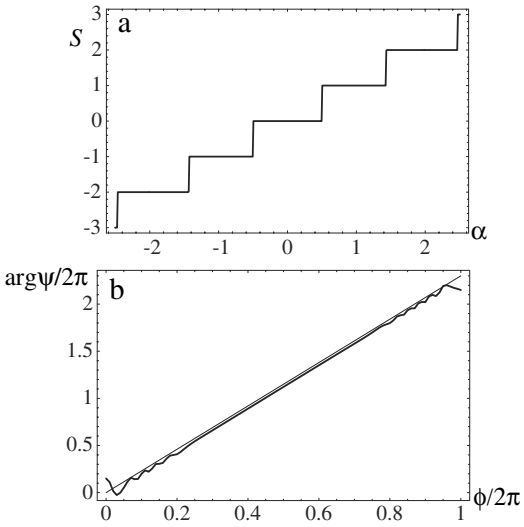

Figure 8. (a) The total vortex strength S (topological charge) of the paraxial wave as a function of α, computed from (19) for $\rho = 3$, showing jumps at half-integer values. (b) Thick curve, the development of integer phase change around a circuit $\rho = 8$ enclosing all vortices, for $\alpha = 2.3$; thin line, the approximation $\alpha\phi$ (equation (21)), that would give a noninteger phase change.

The integral can be evaluated numerically (figure 8(a)), immediately suggesting that

$$S_\alpha = \text{nearest integer to } \alpha = \text{int}\left(\alpha + \tfrac{1}{2}\right). \tag{22}$$

This relation was anticipated on the basis of an analogy with the Aharonov–Bohm effect, as will be explained in section 4. As justification, we first note that (cf (12)) $P_n \to 1$ for large R, so the trigonometric sum in (21) can be evaluated, provided $\phi \neq 0$, with the result

$$\psi_\alpha(\mathbf{r}) \underset{R\to\infty}{\to} \exp(\mathrm{i}(z + \alpha\phi)) \qquad (\phi \neq 0), \tag{23}$$

which also follows from (19) or (20).

Taken by itself, (23) would imply a fractional vortex strength α, which is impossible. But (23) does not apply along the positive x axis, where, as follows from (19), the leading-order behaviour is

$$\psi_\alpha(R \gg 1, \phi = 0, z) = \exp\{\mathrm{i}(z + \alpha\pi)\}\cos(\alpha\pi). \tag{24}$$

This implies that on the positive x axis $\arg\psi_\alpha$ is $\alpha\pi$, up to a multiple of 2π, and the simplest phase assignment that accommodates this with (23) (that is, with the smallest excursion of $\arg\psi_\alpha$ round a closed loop) is

$$\begin{gathered} \alpha = m + \mu \qquad \left(|\mu| < \tfrac{1}{2}\right), \\ \arg\psi_\alpha(R \gg 1, \phi = 0_+) = \mu\pi, \\ \arg\psi_\alpha(R \gg 1, \phi = 2\pi_-) = 2\pi\alpha - \mu\pi, \\ \text{i.e. } \Delta\arg\psi_\alpha = 2\pi(\alpha - \mu) = 2\pi m. \end{gathered} \tag{25}$$

Of course the foregoing is a suggestive argument rather than a proof. Nevertheless, numerical explorations (e.g. figure 8(b)) confirm that the change in $\arg\psi_\alpha$ round a large loop does conform to (25).

3.3. Vortices near the z axis

There are S_α vortices, but where are they? For α close to an integer m, that is $\alpha = m + \mu$, where $|\mu| \ll 1$, it is natural to expect that they lie near the z axis. In (17), the principal contributions for small μ come from the terms $n = m$ and 0, that is

$$\psi_{m+\mu}(\mathbf{r})\exp(-\mathrm{i}z) \underset{\mu\to 0}{\to} \frac{\mu}{m} + \exp\left(\mathrm{i}m\left(\phi - \frac{1}{4}\pi\right)\right)\frac{\sqrt{\pi}}{\Gamma(\frac{1}{2}(m+1))}\left(\frac{\rho^2}{8}\right)^{1/m}. \tag{26}$$

This vanishes at the points

$$\rho = \sqrt{8}\left(\frac{\mu\Gamma(\frac{1}{2}(1+m))}{m\sqrt{\pi}}\right)^{1/m}, \qquad \phi = \pi\left(\frac{2j+1}{m} + \frac{1}{4}\right) \quad (j = 1, 2 \ldots m), \tag{27}$$

confirming that there are m (= nearest integer to α) vortices near the z axis, at the vertices of a regular m-gon; it is easy to see from (26) that they all have the same sign.

3.4. Vortices near the positive x axis for a half-integer step

The nearest integer to α increases by unity when α passes a half-integer, so an extra vortex must be born. To uncover the mechanism of the birth, it is necessary to study the half-integer phase step in more detail, close to the positive ξ axis where the additional vortices are suspected to be. From (19), it follows that

$$\begin{aligned} \psi_{m+\frac{1}{2}}(\xi \gg 1, |\eta| \ll 1, z) &= \mathrm{i}\exp\left\{\mathrm{i}\left(z + \frac{1}{4}\pi\right)\right\}\frac{(m+\frac{1}{2})}{\xi} \\ &\times \left[\sqrt{\frac{2}{\pi}} + \frac{(-\mathrm{i})^{m+1}}{\xi}\exp\left(\frac{1}{2}\mathrm{i}\xi^2\right)\right] \\ &+ \eta\sqrt{\frac{2}{\pi}}\exp\left\{\mathrm{i}\left(z - \frac{1}{4}\pi\right)\right\}. \end{aligned} \tag{28}$$

On the axis ($\eta = 0$), the interference between the two terms gives a steady decay, modulated by oscillations, as illustrated in figure 7(c).

The oscillations hint at the existence of zeros near the axis, and indeed (28) predicts an infinite chain of zeros of $\psi_{m+1/2}$ close to the positive ξ axis, whose positions are

$$\begin{aligned} \xi_n &= \sqrt{2\pi\left(n + \tfrac{1}{2}(m+1)\right)} \qquad (n = 0, 1, \ldots) \\ \eta_n &= \frac{(m+\frac{1}{2})}{\xi_n}\left(1 + \sqrt{\frac{\pi}{2}}\frac{(-1)^n}{\xi_n}\right). \end{aligned} \tag{29}$$

Figure 9 shows how accurately these zeros are located by this asymptotic formula, even for small ξ.

The strength s_n of the nth zero in the chain is the sign of $\mathrm{Im}(\partial_x\psi^*_{m+1/2}\partial_y\psi_{m+1/2})$, and can be calculated from (28); the result is $s_n = (-1)^n$. Thus for $\alpha = m + 1/2$ the vortices in the chain alternate in sign. The chains can be seen in figures 10(b) and 11(b). For the zero closest to the z axis in this chain, $s_0 = +1$; this is the zero that is implicated in the transition between $S_\alpha = m$ and $m + 1$ as α passes through $m + 1/2$, as will be explained in the next section.

An infinite chain of alternating-sign vortices for $\alpha = 1/2$, persisting into the far field, is also described in [4] for the case

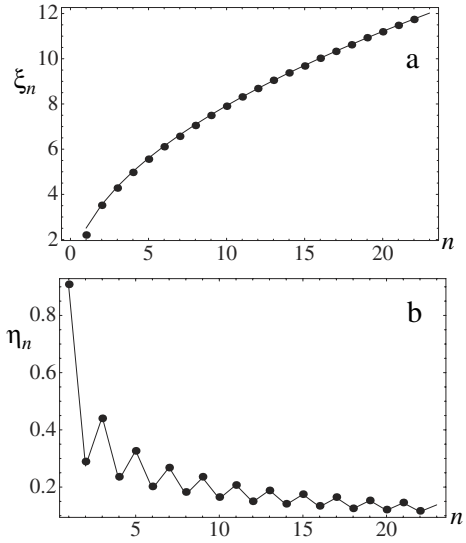

Figure 9. Positions of zeros close to the positive x axis. (a) ξ_n; (b) η_n. The points are computations from the paraxial wave (17), and the curve connects points calculated from the approximation (29).

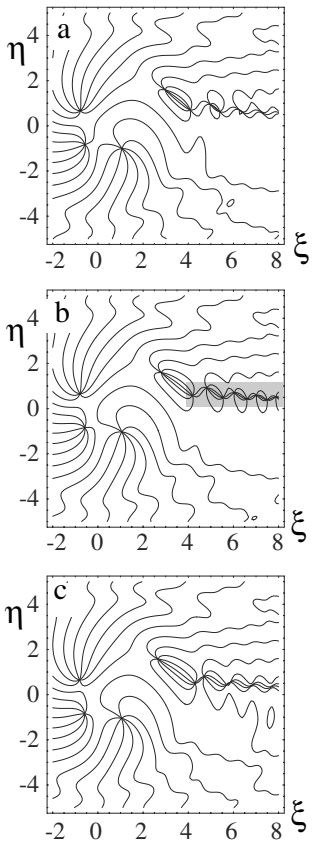

Figure 10. The change of vortex topology from $S = 3$ to 4 near $\alpha = 7/2$, for (a) $\alpha = 3.46$; (b) $\alpha = 3.5$; (c) $\alpha = 3.54$.

of illumination by a beam of finite width, and it is pointed out that most of these lie in regions where the beam is very faint (i.e. large ρ) and so are hard to observe. This is correct, but the vortex chain for a finite beam is different from that generated by plane-wave illumination, in ways I will describe elsewhere.

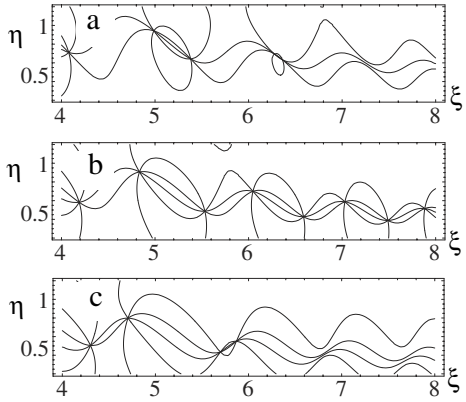

Figure 11. As figure 10, showing magnifications of the shaded area in figure 10(b). For $a = 7/2 + \nu$, the patterns of annihilation of vortices near the positive ξ axis are different for negative ν (a) and positive ν (c).

3.5. The change in vortex topology as α passes through a half-integer

Near a half-integer step, that is $\alpha = m + 1/2 + \nu$, with $|\nu| \ll 1$, the wave acquires an additional term that can be obtained from (23):

$$\psi_{m+\frac{1}{2}+\nu}(\xi \gg 1, \eta \ll 1, z) = \psi_{m+\frac{1}{2}}(\xi \gg 1, \eta \ll 1, z) - \mathrm{i}\pi\nu \exp(\mathrm{i}\pi z) \qquad (|\nu| \ll 1). \tag{30}$$

The condition for the ξ coordinates of the zeros in (29) is now modified, and $\mathrm{Im}[\psi_\alpha \exp(\mathrm{i}\pi/4)] = 0$ gives

$$\frac{\pi\nu}{\sqrt{2}} = \frac{(m+\frac{1}{2})}{\xi^2}\cos\left(\frac{1}{2}(\xi^2 - m\pi)\right). \tag{31}$$

This can be satisfied only if

$$\xi^2 < \frac{(m+\frac{1}{2})\sqrt{2}}{\pi|\nu|}, \tag{32}$$

so the chain of zeros near the x axis is now finite. Using $\xi_n \sim \sqrt{(2\pi n)}$, the number of zeros in the chain can be estimated as

$$N \approx \frac{(m+\frac{1}{2})}{\pi^2|\nu|\sqrt{2}}. \tag{33}$$

This result agrees rather well with numerical observations.

We can now understand the mechanism for the birth of a vortex at a half-integer step. As $|\nu|$ deviates from zero, pairs of alternating-sign vortices annihilate and the chain gets shorter. The result of this process is illustrated in figure 10 and the magnification in figure 11. To understand it, consider the sign of the cosine factor in (31). For $\nu < 0$, the cosine is negative between the zeros ξ_{2k} ($s = +1$) and ξ_{2k+1} ($s = -1$), so the zeros annihilate in pairs whose smaller-ξ member has $s = +1$, so all the vortices get annihilated as ν gets more negative; therefore, the total strength for any negative ν corresponds to the zeros close to $z = 0$, that is, $S_\alpha = m$ (section 3.3). For $\nu > 0$, the cosine is positive between the zeros ξ_{2k-1} ($s = -1$) and ξ_{2k} ($s = +1$), so the zeros annihilate in pairs whose smaller-ξ member has $s = -1$; therefore the annihilations as ν increases leave the $s = +1$ vortex $n = 0$ remaining, so $S_\alpha = m + 1$.

4. Analogy with the Aharonov–Bohm effect

Some of the results of this work were anticipated on the basis of a partial analogy with the Aharonov–Bohm (AB) effect in quantum mechanics [6]. The geometry is slightly different in the two cases. Instead of a phase step originating at a singular point in three dimensions, AB is diffraction from a singular line of magnetic flux, which in quantum units has the value α. Particles transported round the flux line acquire a phase $2\pi\alpha$, which can be observed as a fringe shift in the far field of a plane wave scattered by the flux.

The analogy is between the essentially two-dimensional AB wave (diffraction in a plane pierced by the flux line), and the waves diffracted by a phase step, considered in planes with constant $z > 0$, with α corresponding to the height of the phase step at $z = 0$. Instead of the physical singularity at the flux line $\mathbf{R} = 0$, we have phase singularities at the vortices. In AB, the emphasis is generally in the far field, that is, infinitely far from the flux line, but the flux line itself is a vortex [14], whose strength is the nearest integer to α. This observation was the basis on which the same rule was conjectured for the total singularity strength in the diffraction problem considered here.

In AB, as here, the singularity strength increases by unity as α passes through $m + 1/2$. The mechanism in AB is that when $\alpha = m + 1/2$ a nodal line issues from the flux line and reaches to infinity. As α passes $m + 1/2$, each wavefront, that is, each line $\arg\psi = \text{constant}(\text{mod } 2\pi)$, reconnects with its neighbour, a process that has been observed [14] in a water-wave analogue of AB, in which surface ripples are diffracted by a bathtub vortex. AB is a degenerate version of the problem considered here, in the sense that the nodal line for $\alpha = m+1/2$ replaces the infinite chain of vortices, and for general α the total AB vortex strength is concentrated at $\mathbf{R} = 0$.

A variant of the analogy is the representation of AB using Shelankov's gauge [3, 15], where the magnetic vector potential is confined to an infinitely thin half-plane whose edge is the flux line and across which the phase changes by α; in planes pierced by the flux line, this corresponds to a line across which the phase has a step discontinuity.

Acknowledgments

I thank Professor J F Nye for many helpful comments, and Professor S Roux for a stimulating correspondence. My research is supported by the Royal Society.

Appendix A. The derivation of the uniform approximation (13) for Ψ_1

Starting with (5) for $n = 1$, we eliminate the $1/K$ singularity by using the recurrence relation for J_1, replace the two resulting Bessel functions by their trigonometric integral representation and then evaluate the K integral by stationary phase. This gives

$$\begin{aligned}\Psi_1(\mathbf{r}) &= \exp(\mathrm{i}\phi)\frac{R}{4}\int_{-\infty}^{\infty}\mathrm{d}K\,[J_0(KR)+J_2(KR)]\\ &\quad\times\exp\bigl(\mathrm{i}z\sqrt{1-K^2}\bigr)\\ &\approx\exp\left\{\mathrm{i}\left(\phi-\frac{1}{4}\pi\right)\right\}\frac{Rz\sqrt{2\pi}}{4}I,\end{aligned}\tag{A.1}$$

where

$$I=\frac{1}{\pi}\int_0^{\pi}\mathrm{d}\theta\,\frac{(1+\exp(-2\mathrm{i}\theta))}{(z^2+R^2\sin^2\theta)^{3/4}}\exp\bigl(\mathrm{i}\sqrt{z^2+R^2\sin^2\theta}\bigr).\tag{A.2}$$

Following the standard procedure for obtaining uniform approximations, we change from θ to a new variable ϕ, chosen so that the exponent is simple but has the same topology of stationary points as in (A.2). The appropriate mapping is

$$\sqrt{z^2+R^2\sin^2\theta}=A-B\cos 2\phi.\tag{A.3}$$

The constants A and B are fixed by applying this equality at the two stationary points $\theta = \phi = 0$ (or equivalently π) and $\theta = \phi = \pi/2$, giving

$$A=\tfrac{1}{2}(r+z),\qquad B=\tfrac{1}{2}(r-z).\tag{A.4}$$

Thus

$$I=\frac{\exp(\mathrm{i}A)}{\pi}\int_0^{\pi}\mathrm{d}\phi\,g(\phi)\exp(-\mathrm{i}B\cos 2\phi),\tag{A.5}$$

where

$$g(\phi)=\frac{\mathrm{d}\theta\,(\phi)}{\mathrm{d}\phi}\frac{(1+\exp(-2\mathrm{i}\theta(\phi)))}{(z^2+R^2\sin^2\theta(\phi))^{3/4}}.\tag{A.6}$$

Next, we seek a simple form for $g(\phi)$ that respects the symmetry of the integrand. The correct choice,

$$g(\phi)=p_0+p_1\exp(-2\mathrm{i}\phi)+p_2\exp(-4\mathrm{i}\phi)+\sin(2\phi)g_1(\phi),\tag{A.7}$$

is not obvious and will now be explained. The occurrence of the three terms, involving p_0, p_1 and p_2, rather than the usual two (one for each stationary point), is unexpected, and arises from the fact that $g(\phi)$ in (A.6) vanishes at $\phi = \pi/2$, whose leading asymptotic contribution therefore depends on the curvature $g''(\pi/2)$. This corresponds to the scattering term in the geometric approximation (11), which is of lower order than the plane-wave term representing the initial wave. The last term in (A.7), involving g_1, vanishes at the stationary points, and neglecting it constitutes the lowest-order uniform approximation.

Using (A.7) with g_1 neglected, the uniform approximation to (A.5) is

$$I_{\text{uniform}}=\exp(\mathrm{i}A)[p_0J_0(B)-\mathrm{i}p_1J_1(b)-p_2J_2(B)].\tag{A.8}$$

The final step is to calculate the coefficients. This is achieved using the equality (A.7), evaluated at the two stationary points, and also the curvature of g at the stationary point $\phi = \pi/2$ where $g = 0$, since the curvature determines the leading contribution there:

$$\begin{gathered}g(0)=p_0+p_1+p_2,\qquad g\bigl(\tfrac{1}{2}\pi\bigr)=0=p_0-p_1+p_2,\\ g''\bigl(\tfrac{1}{2}\pi\bigr)=4p_1-16p_2.\end{gathered}\tag{A.9}$$

These equations determine the coefficients, and straightforward but lengthy calculations lead to the formulae (14), and thence, using (A.8), to the uniform approximation (13).

It can easily be confirmed that (13) correctly interpolates between the paraxial formula (7) close to the vortex, and the geometrical formula (11) far from the axis. The term involving J_2 is negligible close to the vortex but plays an essential part in the interpolation, by enabling the matching for large R.

Appendix B. The derivation of the uniform approximation (19) for ψ_α when $|\phi| < \pi/2$

We start with the Huygens–Fresnel integral representation for the paraxial wave propagating from (2), namely

$$\begin{aligned}\psi_\alpha(\mathbf{r}) &= \frac{-\mathrm{i}\exp(\mathrm{i}z)}{2\pi z}\\ &\quad\times \int\!\!\int_{\mathbf{R}'\ \text{plane}} \mathrm{d}\mathbf{R}'\exp\left\{\mathrm{i}\left(\frac{1}{2z}(\mathbf{R}-\mathbf{R}')^2+\alpha\phi'\right)\right\}\\ &= -\frac{\mathrm{i}}{2\pi}\exp\left\{\mathrm{i}\left(z+\frac{1}{2}\rho^2\right)\right\}\int_0^{2\pi}\mathrm{d}\phi'\exp\{\mathrm{i}\alpha\phi'\}\\ &\quad\times\int_0^\infty \mathrm{d}\rho'\,\rho'\exp\left\{\mathrm{i}\left(\tfrac{1}{2}\rho'^2-\rho\rho'\cos(\phi-\phi')\right)\right\}. \qquad \text{(B.1)}\end{aligned}$$

(This is exactly equivalent to (17).) It will be convenient to change the range of the ϕ' integration as follows:

$$\begin{aligned}&\int_0^{2\pi}\mathrm{d}\phi'\exp(\mathrm{i}\alpha\phi')\cdots\\ &= \int_0^{\pi}\mathrm{d}\phi'\exp(\mathrm{i}\alpha\phi')\cdots+\exp(2\pi\mathrm{i}\alpha)\int_{-\pi}^{0}\mathrm{d}\phi'\exp(\mathrm{i}\alpha\phi')\cdots.\end{aligned} \qquad \text{(B.2)}$$

For $\phi < \pi/2$, the dominant contributions to the ϕ' integral will come from the stationary point $\phi' = \phi$ and the endpoint $\phi' = 0$, for which $\cos(\phi'-\phi) > 0$. We will denote the joint contribution from these two sources by $\psi_{\alpha(1)}$. In addition, there is the wave $\psi_{\alpha(2)}$ scattered from the singularity at $\boldsymbol{\rho}' = 0$; this will be considered later.

The ρ' integral in (B.1) is dominated by the stationary point on the positive real axis, giving

$$\begin{aligned}\psi_{\alpha(1)}(\mathbf{r}) &\approx \frac{\rho}{\sqrt{2\pi}}\exp\left\{\mathrm{i}\left(z+\frac{1}{2}\rho^2-\frac{1}{4}\pi\right)\right\}\\ &\quad\times\left(\int_0^\pi \mathrm{d}\phi'\exp(\mathrm{i}\alpha\phi')\cos(\phi'-\phi)\right.\\ &\quad\times\exp\left\{-\tfrac{1}{2}\mathrm{i}\rho^2\cos^2(\phi'-\phi)\right\}\\ &\quad+\exp(2\pi\mathrm{i}\alpha)\int_{-\pi}^{0}\mathrm{d}\phi'\exp(\mathrm{i}\alpha\phi')\cos(\phi'-\phi)\\ &\quad\left.\times\exp\left\{-\tfrac{1}{2}\mathrm{i}\rho^2\cos^2(\phi'-\phi)\right\}\right). \qquad \text{(B.3)}\end{aligned}$$

To determine the large-ρ asymptotics of these angular integrals, we treat the exponential involving ρ^2 as fast-varying, and apply the method of uniform approximation for integrals involving a saddle-point and an endpoint (see for example the appendix to [16]) to map the exponent onto the simplest function with the same qualitative behaviour, with a new integration variable X:

$$\tfrac{1}{2}\rho^2\cos^2(\phi'-\phi) = \tfrac{1}{2}\rho^2+X^2, \qquad \text{i.e. } X = \rho\sin(\phi'-\phi). \qquad \text{(B.4)}$$

Thus

$$\begin{aligned}&\phi' = \phi \leftrightarrow X = 0 \text{ (saddle)};\\ &\phi' = 0 \leftrightarrow X \equiv X_0 = -\frac{1}{\sqrt{2}}\rho\sin\phi \text{ (endpoint)}.\end{aligned} \qquad \text{(B.5)}$$

In the integrals,

$$\begin{aligned}&\mathrm{d}\phi'\exp(\mathrm{i}\alpha\phi')\cos(\phi'-\phi)\\ &= \mathrm{d}X\left(\frac{\mathrm{d}X}{\mathrm{d}\phi'}\right)^{-1}\exp(\mathrm{i}\alpha\phi')\cos(\phi'-\phi)\\ &\equiv \mathrm{d}X\,g(X) = \mathrm{d}X\,[A+BX+X(X-X_0)g_1(X)],\end{aligned} \qquad \text{(B.6)}$$

where

$$\begin{aligned}A = g(0) &= \sqrt{\frac{2}{\rho}}\exp(\mathrm{i}\alpha\phi),\\ B = \frac{g(0)-g(X_0)}{X_0} &= \frac{2}{\rho^2\sin^2\phi}(\exp(\mathrm{i}\alpha\phi)-1).\end{aligned} \qquad \text{(B.7)}$$

The uniform approximation is obtained by neglecting the term involving g_1, which is chosen to vanish at the stationary point and the endpoint, and replacing the integration limits $\pm\pi$ by $\pm\infty$, because the exponent is large at these points, that will later be incorporated into the contribution from the singularity at $\boldsymbol{\rho} = 0$. Then the use of

$$\begin{aligned}\int_{X_0}^\infty \mathrm{d}X\exp(\mathrm{i}X^2) &= \tfrac{1}{2}\exp(\tfrac{1}{4}\mathrm{i}\pi)\sqrt{\pi}\left[1-\mathrm{erf}\left\{X_0\exp\left(-\tfrac{1}{4}\mathrm{i}\pi\right)\right\}\right]\\ \int_{X_0}^\infty \mathrm{d}X\,X\exp(\mathrm{i}X^2) &= \frac{\mathrm{i}}{2X_0}\exp(\mathrm{i}X_0^2)\end{aligned} \qquad \text{(B.8)}$$

in (B.3), and $\eta = \rho\sin\phi$, leads directly to the first two lines of the formula (19).

Finally, we calculate the contribution $\psi_{\alpha(2)}$, associated with the singularity at $\boldsymbol{\rho} = 0$. The integration over ρ' in (B.1) is dominated by the origin, so the exponent involving $\frac{1}{2}\rho'^2$ can be neglected. In the now elementary ρ' integration it is convenient to introduce a convergence factor $\exp(-\varepsilon\rho')$, to disambiguate the poles in the resulting integral over ϕ', leading to

$$\psi_{\alpha(2)}(\mathbf{r}) \approx -\frac{\mathrm{i}}{2\pi}\int_0^{2\pi}\mathrm{d}\phi'\,\frac{\exp(\mathrm{i}\alpha\phi')}{[\varepsilon+\mathrm{i}\rho\cos(\phi'-\phi)]^2}. \qquad \text{(B.9)}$$

For $\alpha > 0$, which we assume for convenience, the pole above the real axis is the one that contributes; for $|\phi| < \pi/2$ this lies at $\phi' = \phi + 3\pi/2$, leading to

$$\psi_{\alpha(2)}(\mathbf{r}) \approx -\mathrm{i}\frac{\alpha}{\rho^2}\exp\left\{\mathrm{i}\left(z+\frac{1}{2}\rho^2+\alpha\left(\phi+\frac{3}{2}\pi\right)\right)\right\}, \qquad \text{(B.10)}$$

which is the contribution in the fourth line of (19).

For $|\phi| > \pi/2$, the other pole contributes, and the resulting expression for $\psi_{\alpha(2)}$ is (B.10) with the exponent $3\pi/2$ replaced by $\pi/2$. For ϕ close to $\pm\pi/2$ there will be some crossover behaviour, involving the endpoints of the integral (B.9), that will not be studied here.

References

[1] Beijersbergen M W, Coerwinkel R P C, Kristensen M and Woerdman J P 1994 Helical-wavefront laser beams produced with a spiral phaseplate *Opt. Commun.* **112** 321–7

[2] Oemrawsingh S S R, van Houwelingen J A W, Eliel E R, Woerdman J P, Verstegen E J K, Kloosterboer J G and 't Hooft G W 2003 Production and characterisation of spiral phase plates for optical wavelengths *Appl. Opt.* **43** 688–94

[3] Berry M V 1999 Aharonov–Bohm beam deflection: Shelankov's formula, exact solution, asymptotics and an optical analogue *J. Phys. A: Math. Gen.* **32** 5627–41
[4] Vasnetsov M V, Basisty L V and Soskin M 1998 Free-space evolution of monochromatic mixed screw-edge wavefront dislocation *Proc. SPIE* **3487** 29–33
[5] Basisty L V, Pas'ko V A, Slyusar V V, Soskin M and Vasnetsov M V 2003 Synthesis and analysis of optical vortices with fractional topological charges *J. Opt. A: Pure Appl. Opt.* at press
[6] Olariu S and Popescu I I 1985 The quantum effects of electromagnetic fluxes *Rev. Mod. Phys.* **57** 339–436
[7] Roux F S 2003 Optical vortex density limitation *Opt. Commun.* **223** 31–7
[8] Keller J B 1962 The geometrical theory of diffraction *J. Opt. Soc. Am.* **52** 116–30
[9] Chester C, Friedman B and Ursell F 1957 An extension of the method of steepest descents *Proc. Camb. Phil. Soc.* **53** 599–611
[10] Bleistein N 1967 Uniform asymptotic expansions of integrals with many nearby stationary points and algebraic singularities *J. Math. Mech.* **17** 533–59
[11] Kravtsov Y A 1964 Asymptotic solution of Maxwell's equations near caustics *Izv. Vuz. Radiofiz.* **7** 1049–56
[12] Berry M V 1976 Waves and Thom's theorem *Adv. Phys.* **25** 1–26
[13] Berry M V 1969 Uniform approximations for glory scattering and diffraction peaks *J. Phys. B: At. Mol. Phys.* **2** 381–92
[14] Berry M V, Chambers R G, Large M D, Upstill C and Walmsley J C 1980 Wavefront dislocations in the Aharonov–Bohm effect and its water-wave analogue *Eur. J. Phys.* **1** 154–62
[15] Shelankov A 1998 Magnetic force exerted by the Aharonov–Bohm flux line *Europhys. Lett.* **43** 623–8
[16] Berry M V and Tabor M 1976 Closed orbits and the regular bound spectrum *Proc. R. Soc.* A **349** 101–23
[17] Walford M, unpublished private communication